International Journal of Mechanical Sciences 53 (2011) 471–478

Contents lists available at ScienceDirect

International Journal of Mechanical Sciences

journal homepage: www.elsevier.com/locate/ijmecsci

Determination of the Drucker–Prager parameters of polymers exhibiting pressure-sensitive plastic behaviour by depth-sensing indentation

Rocio Seltzer [a,*], Adrian P. Cisilino [b], Patricia M. Frontini [b], Yiu-Wing Mai [a]

[a] Centre for Advanced Materials Technology (CAMT), School of Aerospace, Mechanical and Mechatronic Engineering J07, The University of Sydney, Sydney, Australia
[b] Materials Science and Research Institute (INTEMA), Faculty of Engineering, University of Mar del Plata—CONICET, Mar del Plata, Argentina

ARTICLE INFO

Article history:
Received 28 December 2009
Received in revised form
15 June 2010
Accepted 3 April 2011
Available online 14 April 2011

Keywords:
Depth-sensing indentation
Pressure-sensitive materials
Finite element modelling
Inverse analysis

ABSTRACT

This paper presents a method to determine the Drucker–Prager parameters of pressure-dependant elastic-perfectly plastic polymeric materials by means of the depth-sensing indentation technique. This is achieved via an inverse analysis of the load–displacement data resulting from two tests performed with Berkovich and spherical tips. The well-posedness and the effective range of application of the proposed method are carefully assessed first. Then the method is tested for two elasto-plastic materials with mild initial strain-hardening (HDPE and PMMA), and the results are compared to those measured using conventional tensile and compression tests. It is found that the pressure-sensitivity indices can be accurately predicted, while the yield stress predictions in tension and compression fall within the non-linear portion of the uniaxial stress–strain curves, i.e., inside the region where plastic deformation begins.

1. Introduction

Since the appearance of depth-sensing indentation, great efforts have been dedicated to interpret the load–displacement curves in order to extract the mechanical properties of the indented substrates. Unlike traditional tests, e.g., uniaxial tension and compression, determination of mechanical properties using depth-sensing indentation requires some previous knowledge of the material behaviour.

Regarding the determination of Young's modulus for elastic materials, there is already a widely accepted method developed by Oliver and Pharr [1]. However, many materials depart from the same initial assumptions; hence, specific corrections for the Oliver and Pharr method have been proposed for other cases, such as viscoelasticity [2], excessive plastic deformation [3,4], sharp indentation [5], superhard materials [6] and surfaces with residual stresses [7]. Especially, plastic behaviour is a more complex problem and there is a larger diversity of behaviours. For example, indentation methods have already been developed to characterize the yield response of isotropic [8–13] and anisotropic [14] materials, which respond to the Ramberg–Osgood law, semi-brittle elasto-plastic materials with crack formation during indentation [15], and multilayered composites [16].

The indentation responses of materials exhibiting hydrostatic pressure-sensitive plastic behaviour, as is the case of some ceramics [17,18], bulk metallic glasses [19,20] and polymers [21,22], have also been studied. In general, the plastic behaviour of such materials can be described by the Mohr–Coulomb and Drucker–Prager yield criteria [23–27]. The Drucker–Prager [28] yield criterion is a generalisation of Coulomb's law, which is suitable for soil mechanics where the shear stress required for simple slip is linearly dependant on the normal pressure acting on the slip surface. The Drucker–Prager yield criterion has been successfully used to describe the plastic behaviour of polymers [29]. For example, it explains the slip-line patterns formed around notch tips in epoxies under remote tension and compression [30]. Finite element analyses (FEA) of Berkovich and Vickers indentations of elastic–plastic solids obeying both the Mohr–Coulomb and Drucker–Prager criteria were performed by Giannakopoulos and Larson [18] and Vaidyanathan et al. [19] to study the indentation response of ceramics and bulk metallic glasses. They showed that the indentation depth at a given indentation load decreased with the pressure-sensitivity index of the material due to the enhancement of the mean contact pressure. Narasimhan [31] developed a set of analytical equations to calculate the stress and displacement fields of a tip pressing against a material that responds to the hydrostatic pressure-dependant Drucker–Prager yield criterion.

Despite the above-mentioned research, there is yet no established method to determine the properties of pressure-sensitive plastic materials from the load–displacement curves resulting from depth-sensing indentation tests. This work aims to contribute

* Corresponding author. Present address: E.T.S. de Ingeniería de Caminos, C/ Profesor Aranguren, s/n. 28040, Madrid, Spain.
Tel.: +34 91 549 34 22; fax: +34 91 550 30 47.
E-mail address: rocio.seltzer@imdea.org (R. Seltzer).

0020-7403/$ - see front matter © 2011 Elsevier Ltd. All rights reserved.
doi:10.1016/j.ijmecsci.2011.04.002

towards the development of such a method. Assuming that the materials display an elastic-perfectly plastic behaviour and that its plastic behaviour obeys the Druker–Prager yield criterion, a method is proposed herein to extract the values of two independent material properties from the indentation load–displacement curves. That is, yield points in compression and in tension. The pressure-sensitivity index is given by the ratio of these two parameters.

Three main quantities can be measured in an indentation load–displacement curve: the curvature of the loading curve, the initial slope of the unloading curve and the ratio of residual depth to maximum indentation depth. A relation between these three quantities was analytically derived by Tho et al. [32] for conical indenters. The existence of an intrinsic relation amongst three quantities suggests that only two are independent. Thus, only two of three quantities can be obtained from the load–displacement curve arising from a single test using a given indenter geometry. This means that the inverse analysis of a single load–displacement curve to recover three unknown quantities will yield non-unique combinations of elasto-plastic material properties. Cheng and Cheng [33] and Venkatesh et al. [34] also discussed the uniqueness issue and presented a number of computationally non-unique cases. Hence, the inverse approach proposed in this work to determine the plastic properties of pressure-sensitive polymeric materials uses two indenter geometries. Similar methods have also been developed to evaluate the strain-hardening plastic properties of other materials like metals [9–11].

The plastic properties of high-density polyethylene (HDPE) and polymethylmethacrylate (PMMA) in bulk form are determined using the proposed methodology and compared to those directly measured from the conventional tensile and compression tests.

2. Finite element (FE) simulation

2.1. Material model

The materials used for FEA were assumed to obey the Drucker–Prager yield criterion to behave like elastic-perfectly plastic (i.e., no work hardening) and to have time-independent mechanical reactions. With these assumptions, the mathematical description of the plastic behaviour can be reduced to two independent parameters: the pressure-sensitivity index, $\tan\alpha$, and the yield point in compression σ_c.

The Drucker–Prager yield function is given by [35]

$$\phi(\sigma_{ij}) = \sigma_e + \sigma_m \tan\alpha - (1 - \tfrac{1}{3}\tan\alpha)\sigma_c = 0 \tag{1}$$

where

$$\sigma_m = \frac{1}{3}\sigma_{kk} \text{ and } \sigma_e = \sqrt{3J_2} \tag{2}$$

are the hydrostatic stress and von Mises equivalent stress, respectively.

The pressure-sensitivity index is often expressed in terms of the yield points in tension, σ_t, and in compression, σ_c, such that

$$\tan\alpha = 3\frac{m-1}{m+1} \tag{3}$$

where

$$m = \frac{\sigma_c}{\sigma_t} \tag{4}$$

2.2. Computational model

An axisymmetric FE model was developed to simulate the indentation response of elasto-plastic pressure-sensitive materials using the FEA software ABAQUS/Standard [36] (see Fig. 1).

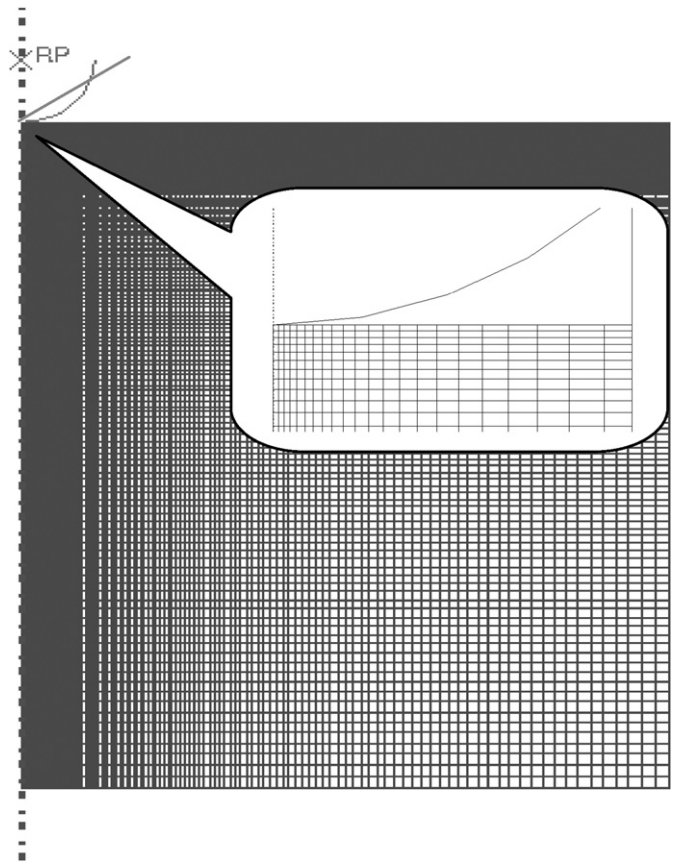

Fig. 1. Axisymmetric finite element model for Berkovich and spherical indentation simulations.

The sample size was set thirty times higher and wider than the indentation depth. A convergence analysis was first performed to assess the dependence of the results with the model discretisation. Hence, it was found that a mesh constructed using 15,000 four-noded quadrilateral elements (CAX4R) with refinement towards the contact zone provides mesh-independent results. The element size in the contact zone was set 100 times smaller than the indenter radius (see Fig. 1). The contact between the indenter and the mesh was assumed frictionless. The indenter was modelled as an analytic surface. Finite deformation formulation was used for all simulations.

Two indentation geometries were simulated: Berkovich (triangular pyramid with a face angle of 80°) and spherical. One of the advantages of these two geometries is that the plastic response is almost unaffected by friction [9,37].

For the conical indenter, the projected contact area is $a = \pi h^2 \cot^2\beta$, where β is the angle between the substrate and the cone. In particular, for a Berkovich indenter, $a = 24.56h^2$. In this study, the 3D geometry of the Berkovich indenter was assimilated in the axisymmetric models to a conical one for which the projected area/depth ratio was identical to that of the Berkovich indenter. This yielded an apex angle of the equivalent cone $\pi/2 - \beta = 70.3°$. This same procedure has been used by other investigators [11].

The performance of the FE models were verified by comparing the results to those reported by Dao et al. [11] for the Berkovich indenter and by Cao et al. [10] for the spherical indenter. Excellent agreements were obtained in both cases.

The FE models were used to conduct a comprehensive parametric study for the range of mechanical properties comprising many polymers. In total, 100 FE models were solved. The ranges

of material properties examined are Young modulus $1 \le E \le 5$ GPa, yield point in compression $20 \le \sigma_c \le 400$ MPa and pressure-sensitivity index $0 \le \tan\alpha \le 0.6$ (or $1 \le m \le 1.5$, see Eqs. (3) and (4)). Poisson's ratio is fixed at $\nu = 0.4$. The combination of these properties yields $30 \le E^*/\sigma_c \le 120$, where E^* is the so-called reduced modulus defined by

$$\frac{1}{E^*} = \frac{(1-\nu_i^2)}{E_i} + \frac{(1-\nu_s^2)}{E_s} \tag{5}$$

The subscripts i and s in Eq. (5) refer to the indenter and the substrate, respectively.

3. Experimental tests

Indentation, tension and compression tests were conducted on a high-density pipe-grade polyethylene (HDPE) kindly provided by Repsol YPF [38], and on a commercial-grade polymethylmethacrylate (PMMA). FTIR studies showed that this type of PMMA might have a plasticisation effect on its mechanical properties. Compression moulded sheets were machined into standard dumb-bell shaped specimens (gauge length equal to 50 mm) and rods or rectangular prisms (height equal to 5 mm) to perform uniaxial tensile and compressive tests, respectively.

The mechanical tests were performed with an Instron 5567 testing machine at ambient temperature (20–25 °C). Tensile elongation was measured using an extensometer with a gauge length of 50 mm. Since polymers are strain rate dependant, similar strain rates were applied in all mechanical tests. Thus, tensile tests were conducted at 5 mm/min and compression tests at 0.5 mm/min to obtain similar strain rates. Young's modulus, E, and yield stress in tension and compression, σ_t and σ_c, were determined from the stress–strain curves. In every case, 5 repeated tests were conducted and their results were averaged.

Indentation tests were performed using a fully calibrated UMIS-2000 nano-indenter (CSIRO, Australia). Details of this facility were published elsewhere [39]. The nano-indenter has a displacement resolution 0.1 nm, internal noise uncertainty <0.1 nm, force resolution 0.75 μN and stage registration repeatability 0.2 μm. Berkovich and spherical (20 μm radius) indenters were used to perform the indentations. Loading and unloading rates were chosen to approximate the strain rate of the tensile and compression tests ($\sim 0.0017\ s^{-1}$). A holding time of 30 s after maximum load was applied was used to calculate the elastic modulus. The contact force to detect the surface position was 0.015 mN. Five indentations separated by a distance of 100 μm were made at ambient temperature for each testing condition.

The reduced elastic modulus E^* was calculated using the Oliver–Pharr model [1] from spherical indentations at depths smaller than 2 μm to avoid excessive errors due to pile-up. To eliminate the creep effects, the indentation stiffness value, S, was corrected with the formula developed by Ngan and Tang [3].

4. Forward analysis

4.1. Single indentation test: non-unique solution

Numerical modelling showed that the indentation tests of two materials with different sets of plastic properties (σ_c and $\tan\alpha$) can yield the same loading–unloading curve. This non-uniqueness of the results is shown in Fig. 2 for the cases of a pressure-sensitive material, with $E = 5$ GPa, $\sigma_c = 60$ MPa and $\tan\alpha = 0.39$, and a pressure-insensitive material, with $E = 5$ GPa, $\sigma_c = 140$ MPa and $\tan\alpha = 0$, tested using a Berkovich indenter. The corresponding developments of the plastic zones at identical indentation depths are

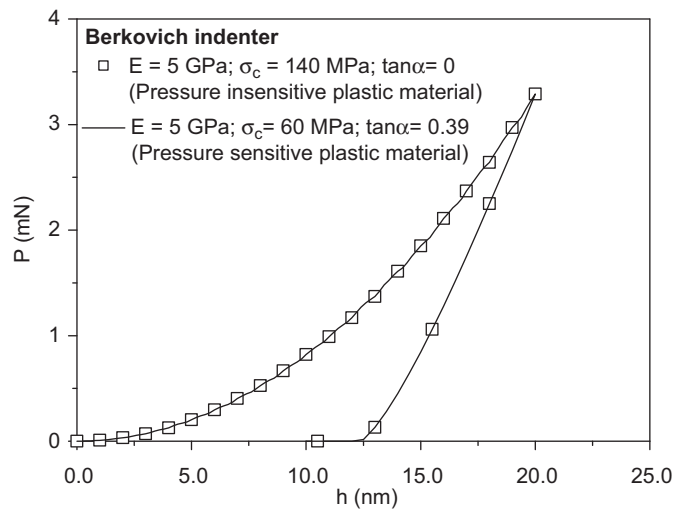

Fig. 2. Loading–unloading curves obtained from simulation of Berkovich indentations of a pressure-sensitive and a pressure-insensitive plastic material. The coincidence in the curves shows the non-uniqueness in the indentation response.

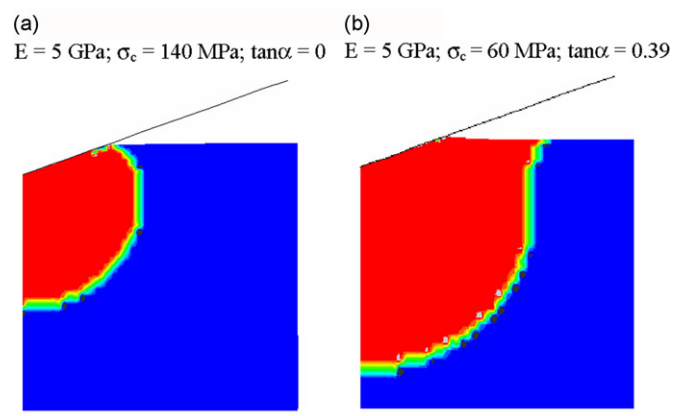

Fig. 3. Plastic zones developed for a Berkovich indenter: (a) pressure-insensitive and (b) pressure-sensitive plastic materials.

shown in Fig. 3. It can be seen that despite the coincidence of the loading–unloading curves for both materials, their plastic zones are significantly different. While the pressure-insensitive material flows only underneath the indenter tip, the plastic zone of the pressure-sensitive material spreads to the free surface. Furthermore, the plastic zone of the pressure-sensitive material is larger than that of the pressure-insensitive material. Hence, it is expected that indentations made with another tip geometry, which would generate a different stress field, will provide two distinct load–displacement curves. With this aim, spherical indentations on both materials were simulated. The results are plotted in Fig. 4, where it is clear that spherical indentation does yield two different load–displacement responses.

Conversely, it was found that two pairs of σ_c and $\tan\alpha$ values that yield identical load–displacement curves for the spherical indentations can show different load–displacement curves for the Berkovich indentations. One of these cases is illustrated in Fig. 5.

4.2. Yield point

If the mechanical behaviour of an elastic-perfectly plastic material is completely defined in terms of the reduced modulus, E^*, and the yield point, σ_y, the load P in Berkovich and spherical

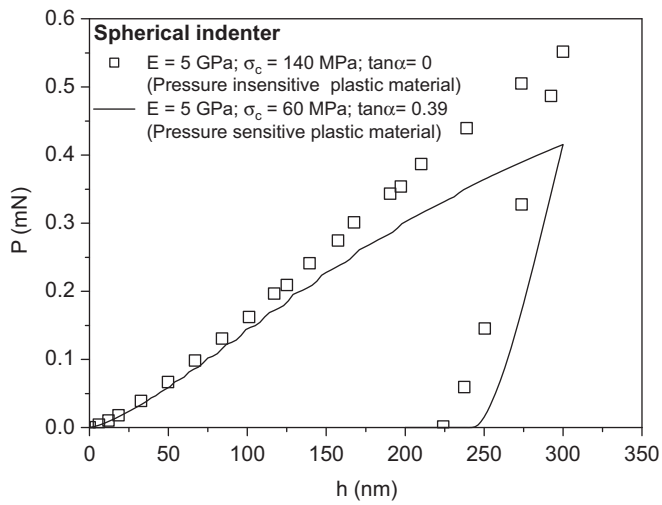

Fig. 4. Loading–unloading curves obtained from simulation of spherical indentations of the same pressure-sensitive and pressure-insensitive plastic materials shown in Fig. 2. In this case there is no coincidence between the indentation responses.

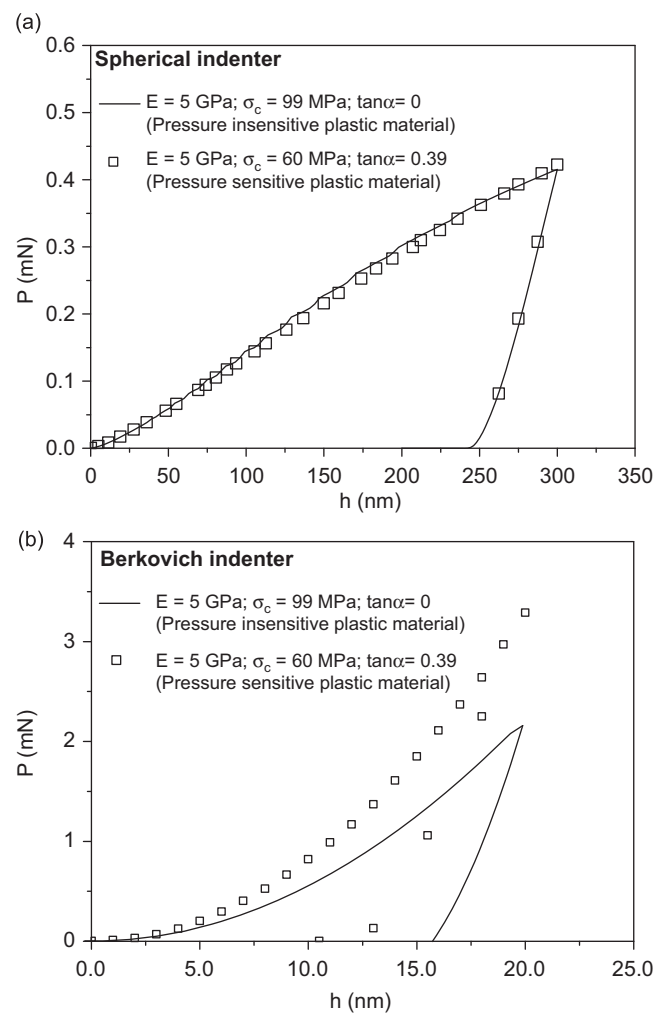

Fig. 5. Loading–unloading curves obtained from simulation of (a) spherical and (b) Berkovich indentations of a pressure-sensitive and a pressure-insensitive plastic material. The results show the non-uniqueness of spherical indentation response.

indentation tests can be expressed, respectively, as

$$P = P(E^*, \sigma_{y(Berkovich)}, h, \beta) \tag{6}$$

and

$$P = P(E^*, \sigma_{y(spherical)}, h, R) \tag{7}$$

By applying the Π theorem in dimensional analysis to Eq. (6) this gives

$$P = \sigma_{y(Berkovich)} h^2 \prod_1^{Berkovich}\left(\frac{E^*}{\sigma_{y(Berkovich)}}, \beta\right) \tag{8a}$$

which is more conveniently expressed by

$$C_i = \frac{P}{h^2} = \sigma_{y(Berkovich)} \prod_1^{Berkovich}\left(\frac{E^*}{\sigma_{y(Berkovich)}}, \beta\right) \tag{8b}$$

Similarly, for Eq. (7), this yields

$$P = \sigma_{y(spherical)} h^2 \prod_1^{spherical}\left(\frac{E^*}{\sigma_{y(spherical)}}, \frac{h}{R}\right) \tag{9}$$

The equations for the functions $\prod_1^{Berkovich}$ and $\prod_1^{spherical}$ that relate P to h, E^*, $\sigma_{y\ (Berkovich)}$ and $\sigma_{y\ (spherical)}$ are given in Appendix A.

4.3. Pressure-sensitivity index and yield point in compression

It has been stated in Section 4.1 that for each pressure-dependant material whose plastic behaviour can be described by σ_c and tan α, there is a pressure-independent material, which yields the same load–displacement response for the same indentation test. Consider, for example, the case illustrated in Fig. 2. The pressure-dependant material with $\sigma_c = 60$ MPa and tan α = 0.39 has the same Berkovich indentation response as the pressure-independent material with $\sigma_c = 140$ MPa and tan α = 0. Hence, $\sigma_{y(Berkovich)} = 140$ MPa. However, there are potentially infinite (σ_c, tan α) pairs whose $\sigma_{y(Berkovich)} = 140$ MPa. In order to determine a function that relates $\sigma_{y(Berkovich)}$ to the pairs (σ_c, tan α) that yield the same indentation behaviour, 50 FE models with different combinations of materials properties were solved. These results are reported in Fig. 6, where the values of the ratio $\sigma_{y(Berkovich)}/\sigma_c$ that yield the same P–h response in Fig. 2 are plotted as a function of tan α for different E^*/σ_c values.

The curves in Fig. 6 can be fitted to a function, tan α, of the following form:

$$\tan\alpha = A^{-1} \ln\left(\frac{\sigma_{y(Berkovich)}}{\sigma_c}\right) \tag{10}$$

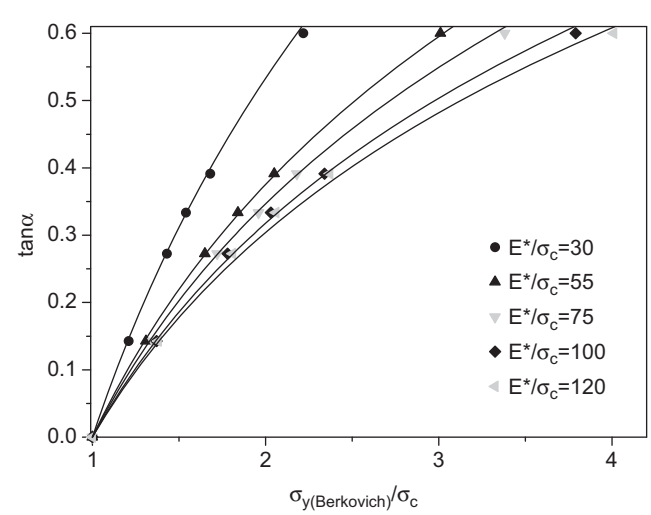

Fig. 6. tan α versus $\sigma_{y(Berkovich)}/\sigma_c$ plot for different E^*/σ_c ratios representing the group of values (σ_c, tan α, E^*, $\sigma_{y(Berkovich)}$) for which the Berkovich indentation responses are identical.

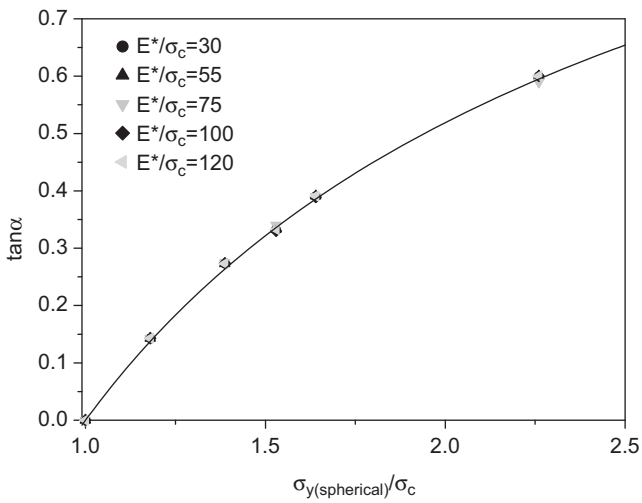

Fig. 7. tan α versus $\sigma_{y(spherical)}/\sigma_c$ plot representing the group of values (σ_c, tan α, $\sigma_{y(spherical)}$) for which the spherical indentation responses are identical. In contrast to Berkovich indentations, the shape of the curve is independent of E^*/σ_c.

where A is given by

$$A = -0.52627\ln\left(\frac{E^*}{\sigma_c}\right) + 0.41239\left[\ln\left(\frac{E^*}{\sigma_c}\right)\right]^2 - 0.042340\left[\ln\left(\frac{E^*}{\sigma_c}\right)\right]^3 \tag{11}$$

The above fit predicts $\sigma_{y(Berkovich)}/\sigma_c$ values within 3.5% error from the FEA solutions.

As for the Berkovich indenter, a function that relates the pairs (σ_c, tan α) that yield the same indentation curve can be found for the spherical indenter (see Fig. 7). This is

$$\tan\alpha = 0.87444\ln\left(\frac{\sigma_{y(spherical)}}{\sigma_c}\right) - 0.16419\left[\ln\left(\frac{\sigma_{y(spherical)}}{\sigma_c}\right)\right]^2 \tag{12}$$

However, unlike the Berkovich indentations, it is noted that the function, tan α, for spherical indentations is independent of $E^*/\sigma_{y(spherical)}$.

5. Inverse analysis

5.1. Algorithm

Based on the results and relations given in Section 4, an algorithm for the determination of E^*, σ_c and tan α for pressure-sensitive plastic materials is presented next. The input data are the P–h curves for three indentation tests:

- loading curve of the Berkovich test with a relative indentation depth up to $h/R=0.1$;
- loading curve of a spherical-tip test with a relative indentation depth up to $h/R=0.1$ and
- the load–hold–unload curve of a spherical-tip test with a relative depth $h/R<0.1$.

Step 1: Compute the reduced modulus E^* by means of the Oliver–Pharr [1] model and the Ngan and Tang [3] correction for creep using the data from the load–hold–unload P–h test with the spherical tip.

Step 2:

- Fit the P–h curve of the Berkovich indentation test using a function of the form $P=C_ih^2$ to determine C_i.
- Compute $\sigma_{y(Berkovich)}$ using Eq. (A.1) and E^* obtained in *Step 1*.

Step 3:

- Determine the load at $h=0.1R$ from the P–h curve of the indentation test performed with the spherical tip.
- Compute $\sigma_{y(spherical)}$ using Eq. (A.2) and E^* obtained in *Step 1*.

Step 4:

- Set up a system of equations using Eqs. (10) and (12) with values of E^*, $\sigma_{y(Berkovich)}$ and $\sigma_{y(spherical)}$ determined in the previous steps.
- Solve the system of equations to find σ_c and tan α using the Newton method.
- Use Eqs. (3) and (4) to determine σ_t.

5.2. Effectiveness of the algorithm

A first point to consider when using the above proposed algorithm is its application range. It must be noted that the range of properties analysed to develop the algorithm is $30<E^*/\sigma_c<120$ and $0<\tan\alpha<0.6$ (or $1<m<1.5$). Thus, solutions outside this range are not reliable.

Another issue that must be considered is the well-posedness of the inverse problem. According to Hadamard [40], a problem is well-posed if the following conditions are satisfied:

- a solution exists (existence);
- the solution is unique (uniqueness) and
- the solution depends continuously on the problem data (stability).

In particular, the last condition means that a small change in the problem data does not cause an abrupt, disproportionate change in the solution. This property is especially important for inverse analyses, since perturbations arising from measuring inevitable errors, such as those in experimental data. Discussion on the satisfaction of the above conditions for the problem is next given, and the range of properties where this method yields reliable results is established.

5.2.1. Existence and uniqueness

The existence and uniqueness of the solutions were checked for the outputs of the 100 FE models cases solved in Section 2. In every case the algorithm returned the values of the prescribed mechanical property values accurately. It should be noted that the solutions of the system given by Eqs. (10) and (12) must be found always within the limits of the interpolations:

$$1 \le \frac{\sigma_{y(spherical)}}{\sigma_c} \le 2.25 \tag{13}$$

and

$$1 \le \frac{\sigma_{y(Bercovich)}}{\sigma_c} \le 4 \tag{14}$$

5.2.2. Stability

The stability analysis assesses the sensitivity of the results to small perturbations in the input values. The stability of a problem can be assessed by means of the condition number κ (see Appendix B). The better conditioned is a problem, the closer κ is to 1. The function κ is plotted in Fig. 8 within the analysed range for the input variables, which is $30 \le E^*/\sigma_c \le 120$ and $1 \le (\sigma_{y(spherical)}/\sigma_c) \le 2.25$. It can be seen that the stability of the method deteriorates rapidly

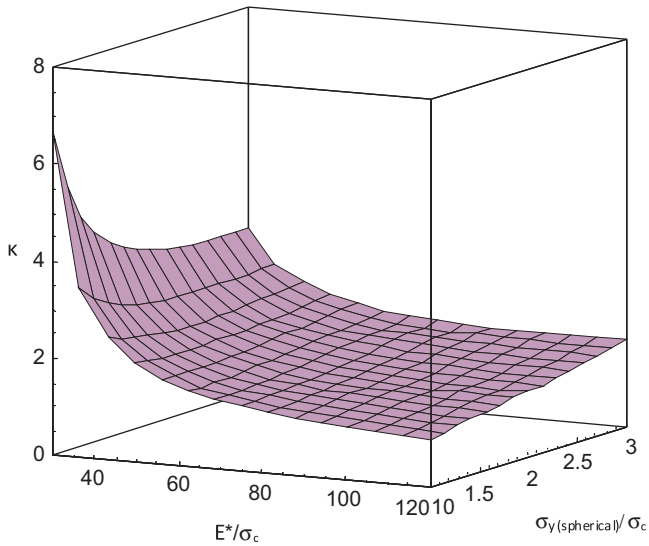

Fig. 8. Condition number, κ, as a function of dimensionless mechanical properties for the inverse problem studied.

when $E^*/\sigma_c < 40$. In such a case, the sensitivity to errors in the input data also increases when $\sigma_{y(spherical)}/\sigma_c$ decreases, i.e., when the material yield point has a weak dependence on pressure. In contrast, the method is well-posed in all the range of $\sigma_{y\ (spherical)}/\sigma_c$ when $E^*/\sigma_c > 40$.

The physical explanation for the deterioration in the well-posedness of the method is that as E^*/σ_c decreases, the indentation response tends to be more elastic, and hence its plastic properties are more difficult to identify. In such a case, a means to extend the application range of the method would be to use combinations of more acute indenters (like conical indenters with apex angles less than 70.3°) to develop larger plastic zones under the indenter tip. However, cautions must be exercised because some experimental difficulties may arise, such as the influence of friction in the indentation response and the roundness of the indenter tip.

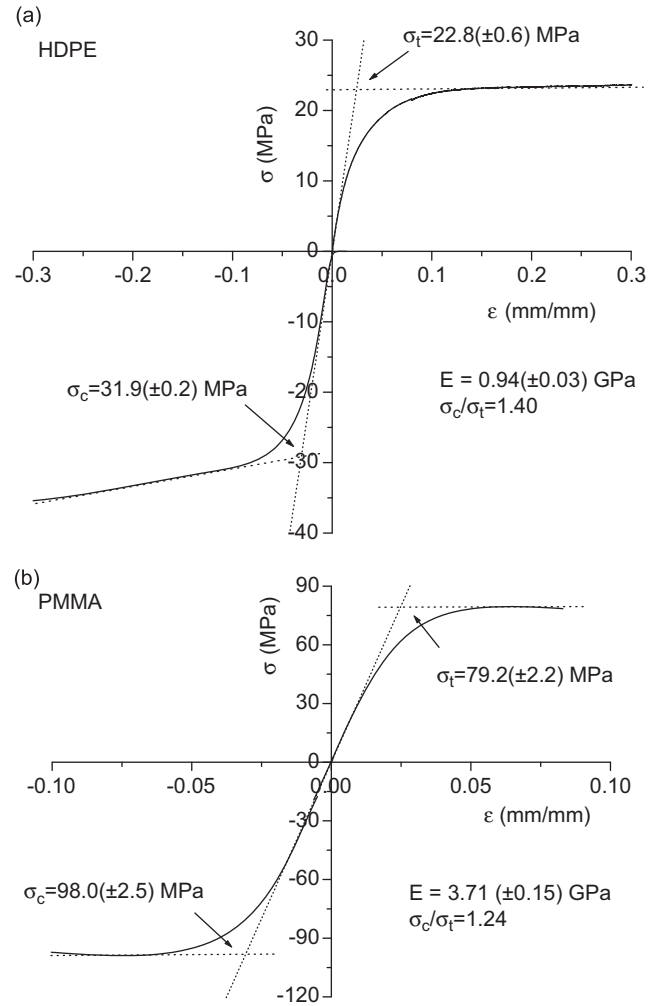

Fig. 9. Typical true stress/true strain curves obtained from tensile and compression tests for (a) HDPE and (b) PMMA.

6. Applications to PMMA and HDPE

6.1. Experimental results

Typical true stress–true strain curves for HDPE and PMMA (see Section 3) in tension and compression are shown in Fig. 9. Young's moduli, E, were calculated from the initial slope for both materials. The points on the curves where plastic deformation begins are within the ranges delimited by the initial departure from linearity and the maximum stress. It is a common practice in polymers to assimilate the yield stress to the maximum stress [41]. Alternatively, in absence of a maximum stress, as it is in the case of the compression curve of HDPE (see Fig. 9(a)), the yield stress may be obtained from the intersection of the straight lines, which result from the linear extrapolations of the elastic and post-yield portions of the true stress–true strain curve. The yield stresses in tension, σ_t, and compression, σ_c, were hence determined for both materials using the previously described procedure.

Typical P–h curves resulting from the indentation tests on HDPE and PMMA using the Berkovich and spherical tips are plotted in Fig. 10 (shown as continuous curves).

6.2. Application of the inverse method

The inverse problem in Section 5 assumes an elastic-perfectly plastic material behaviour with a sharp switch between the initial elastic regime and the plastic plateau. However, as shown in Fig. 9, both HDPE and PMMA present a smooth and gradual transition between their elastic responses and the plastic plateaus. Moreover, it can also be argued that these smooth transitions represent the strain-hardening behaviour of the materials. The determination of the strain-hardening parameter would require an extra loading curve for an indentation made with a third tip geometry. Hence, a modified inverse method would be required. Such a method based on the indentation results of three indenter geometries would not only be more arduous to implement, but it would be applicable only to a specific stress–strain response, which should be known *a priori*. Therefore, strain-hardening was neglected in the present analysis, giving priority to practicality over accuracy.

The material properties determined from the experimental P–h curves in Fig. 10 using the algorithm introduced in Section 5.1 are given in Table 1. In both cases, the solution procedure was well-conditioned, with $E^*/\sigma_c \approx 79$ and $E^*/\sigma_c \approx 60$ for HDPE and PMMA, respectively. The indentation elastic moduli, E, and the pressure-sensitivity index, σ_c/σ_t, given in Table 1 agree quite well (within 13% and 5% error, respectively) with those values measured directly from the tension and compression tests shown in Fig. 9. Further, the yield stresses in tension and compression obtained from the inverse method are always within the range between the initial departure from linearity and maximum stress in the uniaxial tests (see Section 6.1).

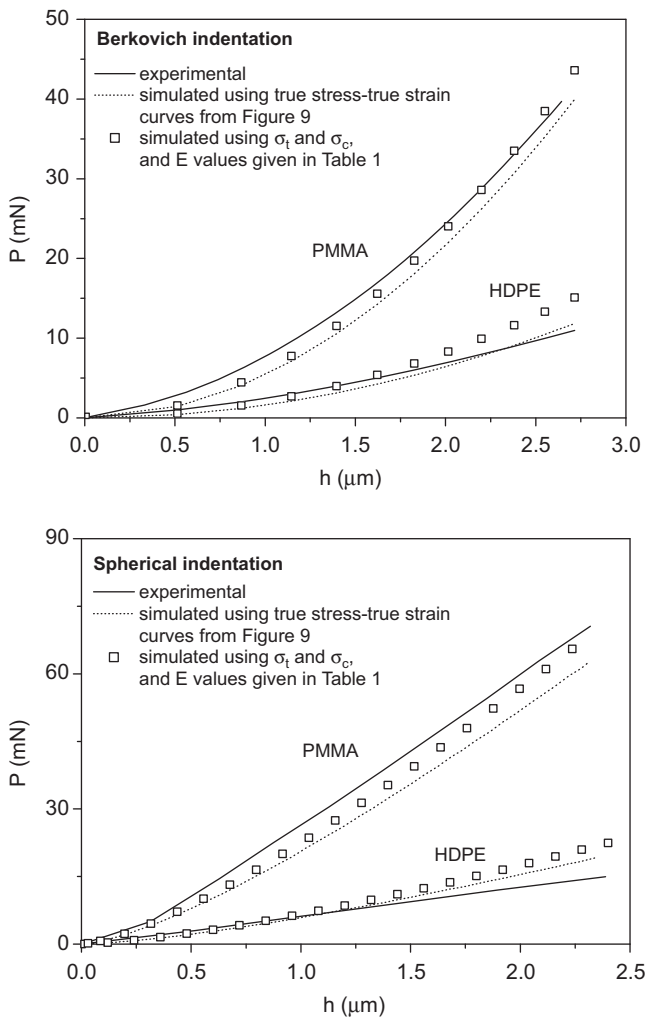

Fig. 10. Experimental and simulated *P–h* curves for HDPE and PMMA due to Berkovich and spherical indentations.

Table 1
Mechanical properties of HDPE and PMMA determined from experimental *P–h* curves using the inverse method proposed in Section 5.1.

	E (GPa)[a]	σ_c (MPa)	σ_t (MPa)	σ_c/σ_t
HDPE	1.08 ($\pm$0.08)	17.1	12.8	1.34
PMMA	4.09 ($\pm$0.03)	81.1	62.2	1.30

[a] To calculate E, the Poisson ratio was taken from published data assuming $\nu=0.45$ for HDPE (Lai J, PhD thesis, Delft University, 1995) and $\nu=0.4$ for PMMA (http://www.goodfellow.com/).

An interesting question may be asked. Are the indentation curves simulated using two sets of material properties for HPDE and PMMA: (a) actual experimental stress versus strain responses in Fig. 9 and (b) assumed elastic-perfectly plastic behaviours with material constants (E, σ_c and σ_t) given in Table 1 similar? Fig. 10 plots these simulated *P–h* curves, which show good agreement with each other for both materials confirming the equivalency of the two set of inputs.

Naturally, if the simulated indentation curves in Fig. 10 are used to obtain the plastic properties using the inverse method in Section 5.1, such as those shown in Table 2, they should be similar to the (E, σ_c and σ_t) values in Table 1, which are derived from the experimental indentation curves. Indeed they are.

Table 2
Plastic properties of HDPE and PMMA determined from the simulated curves shown in Fig. 10 using the inverse method proposed in Section 5.1.

Depth-sensing indentation (simulated)					
	σ_c (MPa)	σ_t (MPa)	σ_c/σ_t	$\sigma_{y(Berkovich)}$ (MPa) [11]	$\sigma_{y(spherical)}$ (MPa) [10]
HDPE	20.4	14.9	1.37	48.3	37.5
PMMA	74.5	59.8	1.25	135	112

Also reported in Table 2 are the yield stresses, $\sigma_{y(Berkovich)}$ and $\sigma_{y(spherical)}$, for HPDE and PMMA calculated using the Dao et al. [11] and Cao et al. [10] methods, respectively. It can be seen that these values are much larger than the actual values determined from the tension and compression tests (see Fig. 9). Therefore, there are limitations of the methods proposed by Dao et al. [11] and Cao et al. [10] for pressure-sensitive plastic materials.

7. Conclusions

In has been demonstrated in this work that the Drucker–Prager parameters (pressure-sensitivity index and yield stresses in tension and compression) of pressure-sensitive polymers can be determined by means of depth-sensing indentation using a combination of two different tip geometries and inverse analysis.

An inverse method to determine the Drucker–Prager parameters from indentation *P–h* curves was devised using finite element simulation. The method is effective and can be reliably applied to materials for which the ratio of the reduced modulus to the yield stress in compression is $E^*/\sigma_c > 40$.

The proposed method was tested for two elasto-plastic materials with mild initial strain-hardening, HDPE and PMMA. The pressure-sensitivity index was predicted with an error less than 5%. In every case the predicted yield stresses fell well within the stress range delimited by the initial departure from linearity and the maximum stress in the experimental stress–strain curves. These results are an improvement with respect to the predictions using other schemes and methods, which do not account for the effects of pressure sensitivity and overestimate the yield stresses.

The proposed method can be potentially extended by adding extra tests with different tip geometries (e.g., conical indenters of varying angles). In this way, the method will be applicable to materials with $E^*/\sigma_c < 40$ and/or effect of strain-hardening.

Acknowledgements

The authors thank the Australian Research Council and the Cooperative Research Centre for Advanced Composite Structures for their financial support in this work. The support of the Agencia Nacional de Promoción Científica y Tecnológica (ANPCyT) of Argentina through grant PICT 2997 no. 1154 is also acknowledged.

Appendix A

In the case of Berkovich indentation of elastic-perfectly plastic materials, Dao et al. [11] obtained the following relation:

$$\Pi_1^{Berkovich} = \frac{C_i}{\sigma_{y(Berkovich)}} = 29.267 - 30.596\left[\ln\left(\frac{E^*}{\sigma_{y(Berkovich)}}\right)\right] + 13.635\left[\ln\left(\frac{E^*}{\sigma_{y(Berkovich)}}\right)\right]^2 - 1.131\left[\ln\left(\frac{E^*}{\sigma_{y(Berkovich)}}\right)\right]^3 \quad (A.1)$$

where C_i is the coefficient of the interpolating equation $P = C_i h^2$ of the loading curve in a sharp indentation test.

For spherical indentation of elastic-perfectly plastic materials, when $h = 0.1R$, Cao and Lu [42] found that

$$\prod_1^{spherical} = \frac{P|_{h/R=0.1}}{\sigma_{y(spherical)} h^2} = -64.419 + 25.055\left[\ln\left(\frac{E^*}{\sigma_{y(spherical)}}\right)\right] + 11.500\left[\ln\left(\frac{E^*}{\sigma_{y(spherical)}}\right)\right]^2 - 1.356\left[\ln\left(\frac{E^*}{\sigma_{y(spherical)}}\right)\right]^3 \tag{A.2}$$

Cao et al. [10] have provided a set of similar equations for depths h/R between 0.01 and 0.1. The latter was chosen given its algorithm has the highest stability. This becomes important when the ratio $E^*/\sigma_{(spherical)}$ is small. From a physical point of view, the indentation depth should be sufficient to deform the material plastically.

Appendix B

The condition number is given by

$$Cond(x) = \left|\frac{xf'(x)}{f(x)}\right| \tag{B.1}$$

where x is the input, $f(x)$ the output and $f'(x)$ stands for the derivative of $f(x)$ with respect to x. For a given problem, the inverse problem is to determine what input would yield a given output. For the problem of evaluating a function, $y = f(x)$, the inverse problem, denoted by $x = f^{-1}(y)$, is to determine, for a given value y, a value x such that $f(x) = y$. From the definition, we see that the condition number of the inverse problem, κ, is the reciprocal of that of the original problem:

$$\kappa(x) = \left|\frac{f(x)}{xf'(x)}\right| \tag{B.2}$$

In the analysis carried out in this study:

$$f = \sigma_c e^{A\tan\alpha} \tag{B.3}$$

$$y = \sigma_{y(Berkovich)} \tag{B.4}$$

$$x = \sigma_c \tag{B.5}$$

where A is defined in Eq. (11) and $\tan\alpha$ is replaced by Eq. (12). Hence, the condition number of the inverse problem κ is a function of the reduced modulus, yield point in compression and the reference yield point in the spherical test:

$$\kappa = g\left(\frac{\sigma_{y(spherical)}}{\sigma_c}, \frac{E^*}{\sigma_c}\right) \tag{B.6}$$

References

[1] Oliver WC, Pharr GM. An improved technique for determining hardness and elastic modulus using load and displacement sensing indentation experiments. J Mater Res 1992;7:1564–83.
[2] Tsui TY, Oliver WC, Pharr GM. Influences of stress on the measurement of mechanical properties using nanoindentation: part I. Experimental studies in an aluminum alloy. J Mater Res 1996;11:752–9.
[3] Ngan AHW, Tang B. Viscoelastic effects during unloading in depth-sensing indentation. J Mater Res 2002;17:2604–10.
[4] Tranchida D, Piccarolo S, Loos J, Alexeev A. Accurately evaluating Young's modulus of polymers through nanoindentations: a phenomenological correction factor to the Oliver and Pharr procedure. Appl Phys Lett 2006;89:171905_1.
[5] Shu S, Lu J, Li D. A systematic study of the validation of Oliver and Pharr's method. J Mater Res 2007;22:3385–96.
[6] Fischer-Cripps A. Illustrative analysis of load-displacement curves in nanoindentation. J Mater Res 2007;22:3075–86.
[7] Kese KO, Li ZC, Bergman B. Influence of residual stress on elastic modulus and hardness of soda-lime glass measured by nanoindentation. J Mater Res 2004;19:3109–19.
[8] Chollacoop N, Dao M, Suresh S. Depth-sensing instrumented indentation with dual sharp indenters. Acta Mater 2003;51:3713–29.
[9] Bucaille JL, Stauss S, Felder E, Michler J. Determination of plastic properties of metals by instrumented indentation using different sharp indenters. Acta Mater 2003;51:1663–78.
[10] Cao YP, Dao M, Lu J. A precise correction method for the study the superhard materials using the nanoindentation. J Mater Res 2007;22:1255–64.
[11] Dao M, Chollacoop N, Van Vliet KJ, Venkatesh TA, Suresh S. Computational modeling of the forward and reverse problems in instrumented sharp indentation. Acta Mater 2001;49:3899–918.
[12] Hasanov A. An inversion method for identification of elastoplastic properties for engineering materials from limited spherical indentation measurements. Inverse Prob Sci Eng 2007;15:601–27.
[13] Haj-Ali R, Kim H-K, Koh SW, Saxena A, Tummala R. Nonlinear constitutive models from nanoindentation tests using artificial neural networks. Int J Plast 2008;24:371–96.
[14] Nakamura T, Gu Y. Identification of elastic–plastic anisotropic parameters using instrumented indentation and inverse analysis. Mech Mater 2007;39:340–56.
[15] Zhang H, Fang ZZ, Belnap JD. Quasi-plastic deformation of WC-Co composites loaded with a spherical indenter. Metall Mater Trans A 2007;38:552–61.
[16] Tan XH, Shen Y-L. Modeling analysis of the indentation-derived yield properties of metallic multilayered composites. Compos Sci Technol 2005;65:1639–46.
[17] Zeng K, Soderlund E, Giannakopoulos AE, Rowcliffe DJ. Controlled indentation: a general approach to determine mechanical properties of brittle materials. Acta Mater 1996;44:1127–41.
[18] Giannakopoulos AE, Larsson PL. Analysis of pyramid indentation of pressure-sensitive hard metals and ceramics. Mech Mater 1997;25:1–35.
[19] Vaidyanathan R, Dao M, Ravichandran G, Suresh S. Study of mechanical deformation in bulk metallic glass through instrumented indentation. Acta Mater 2001;49:3781–9.
[20] Fornell J, Concustell A, Surinach S, Li WH, Cuadrado N, Gebert A, Baró MD, Sort J. Yielding and intrinsic plasticity of TiZrNiCuBe bulk metallic glass. Int J Plast 2009;25:1540–59.
[21] Briscoe BJ, Flori L, Pelillo E. Nanoindentation of polymeric surfaces. J Phys D: Appl Phys 1998;31:2395–405.
[22] Briscoe BJ, Sebastian KS. The elastoplastic response of poly(methyl methacrylate) to indentation. Proc R Soc Lond A 1996;452:439–57.
[23] Vena P, Gastaldi D, Contro R. Determination of the effective elastic–plastic response of metal–ceramic composites. Int J Plast 2008;24:483–508.
[24] Aydin I, Briscoe BJ, Sanliturk KY. The internal form of compacted ceramic components: a comparison of a finite element modelling with experiment. Powder Technol 1996;89:239–54.
[25] Donovan PE. A yield criterion for $Pd_{40}Ni_{40}P_{20}$ metallic glass. Acta Metall 1989;37:445–56.
[26] Bowden PB, Jukes JA. The plastic flow of polymers. J Mater Sci 1972;7:52–63.
[27] Quinson R, Perez J, Rink M, Pavan A. Yield criteria for amorphous glassy polymers. J Mater Sci 1997;32:1371–9.
[28] Drucker DC, Prager W. Soil mechanics and plastic analysis of limit design. Appl Math 1952;8:157–62.
[29] Drucker DC. Plasticity theory, strength-differential (SD) phenomenon, and volume expansion in metals and plastics. Metall Trans 1973;4:667–73.
[30] Jeong H-Y, Li X-W, Yee AF, Pan J. Slip lines in front of a round notch tip in a pressure-sensitive material. Mech Mater 1994;19:29–38.
[31] Narasimhan R. Analysis of indentation of pressure sensitive plastic solids using the expanding cavity model. Mech Mater 2004;36:633–45.
[32] Tho KK, Swaddiwudhipong S, Liu ZS, Zeng K, Hua J. Uniqueness of reverse analysis from conical indentation tests. J Mater Res 2004;19:2498–502.
[33] Cheng YT, Cheng CM. Can stress–strain relationships be obtained from indentation curves using conical and pyramidal indenters? J Mater Res 1999;14:3493–6.
[34] Venkatesh TA, Van Vliet KJ, Giannakopoulos AE, Suresh S. Determination of elasto-plastic properties by instrumented sharp indentation: guidelines for property extraction. Scr Mater 2000;42:833–9.
[35] Chen WF, Han DJ. Plasticity for structural engineers. Secaucus, New Jersey: Springer Verlag; 1988.
[36] ABAQUS theory manual version 6.3. Pawtucket: Hibbitt, Karlsson and Sorensen, Inc.; 2002.
[37] Taljat B, Pharr GM. Development of pile-up during spherical indentation of elastic–plastic solids, Int. J Solids Struct 2004;41:3891–904.
[38] Del Amo B, Hernández-Vaquero JL, Segura S, Hernández Borjabad V, Benham EA, McDaniel MP, Seltzer R, Frontini PM. Polietilenos bimodales para la aplicación de tubería. Nuevas rutas para su obtención. Revista de Plásticos Modernos 2002;82:558–70.
[39] Bell TJ, Bendeli A, Field JS, Swain MV, Thwaite EG. The determination of surface plastic and elastic properties by ultra micro-indentation. Metrologia 1991;28:463–9.
[40] Hadamard J. Lectures on Cauchy's problems in linear partial differential equations. New Haven, CT: Yale University Press; 1923.
[41] Cheremisinoff NP. Handbook of polymer science and technology. New York & Basel: Marcel Dekker Inc.; 1989.
[42] Cao YP, Lu J. A new scheme for computational modeling of conical indentation in plastically graded materials. J Mater Res 2004;19:1703–16.